ELSEVIER





# Structural design of a scalable glass with high hardness and crack initiation resistance

**Anjali Yadav [a], Anne Rebecca [a,1], Saurabh Kapoor [a,b], Yueh-Ting Shih [c], Liping Huang [c], Ashutosh Goel [a,*]**

[a] Department of Materials Science and Engineering, Rutgers, The State University of New Jersey, Piscataway, NJ 08854, United States
[b] Centre of Excellence, Sterlite Technologies Ltd, MIDC Waluj, Aurangabad, 431136, India
[c] Department of Materials Science and Engineering, Rensselaer Polytechnic Institute, Troy, NY 12180, United States

**The industry has always strived to design "hard" and "crack-resistant" glass. However, simultaneously realizing these properties in oxide glasses has been rare. Although $Al_2O_3$-rich hard and crack-resistant oxide glasses have been reported in the last decade, they exhibit two significant technological challenges that hinder their translation from laboratory to industry: (1) high processing temperatures (>2000 °C) and (2) small glass-forming regions (near eutectic). The present study reports the structural design of a hard and high modulus glass with high crack initiation resistance designed in the peraluminous region of rare-earth containing $MgO–Al_2O_3–B_2O_3–SiO_2$ system. The glass can be processed at a temperature ≤1650 °C and exhibits Vickers hardness ($H_v$) of 7.84 GPa (at 1.96 N load) and indentation crack resistance (ICR) of 26.5 N. These $H_v$ and ICR values are significantly higher than most commercial or non-commercial glasses (prior to thermal tempering, densification near $T_g$, or chemical strengthening). The glass has been scaled up to successfully produce slabs of dimensions 100 mm × 100 mm × 8 mm at laboratory scale with optical transmission of 90 ± 2 %. The results presented here are scientifically intriguing and have considerable tangible implications, as they pave the path for the design and development of stronger glasses for functional applications.**

**Keywords: Glass; Hardness; Crack resistance; Structure**

## Introduction

The brittleness of glass has been perceived as its gravest handicap. While the glass industry has always strived to design a "hard" and "crack-resistant" glass, simultaneous realization of both these properties in oxide glasses has been challenging and a rare achievement [1,2]. Based on decades of work, it is generally believed that a hard glass with high elastic modulus requires a high packing density and high bond energy components, while a crack resistant glass is expected to exhibit low packing density so that the glasses can be easily compacted by force [3,4]. As an example, a cesium aluminoborate glass with indentation crack resistance (ICR) of ≈500 N (upon aging for 7 days in humid conditions) has been shown to exhibit Vickers hardness ($H_v$) of 2 GPa and Young's modulus (E) of 20 GPa [5]. On the other hand, glasses with high $H_v$, for example, 6–8 GPa, exhibit low ICR, as shown in Fig. 1. Similar correlations between hardness and ICR can be observed in most oxide glasses, as has been discussed in our previous studies [6,7]. However, the notion of an inverse relationship between the hardness and ICR in oxide glasses has been challenged in the recent years wherein, "hard" and "crack resistant" glasses have been developed by Rosales-Sosa et al. [8], i.e., 60 $Al_2O_3$ – 40 $SiO_2$ (mol.%) glass with $H_v$ = 8.07 GPa and ICR = 55.4 N; and Ke et al. [9], i.e., 11.15 MgO – 38.39 $Al_2O_3$ – 50.00 $SiO_2$ (mol.%) glass with $H_v$ = 7.41 GPa and ICR = 50.2 N.

* Corresponding author.
*E-mail address:* Goel, A. (ag1179@soe.rutgers.edu)
[1] Present address: Corning Incorporated, Corning, NY 14830, USA.

1369-7021/ https://doi.org/10.1016/j.mattod.2024.06.009

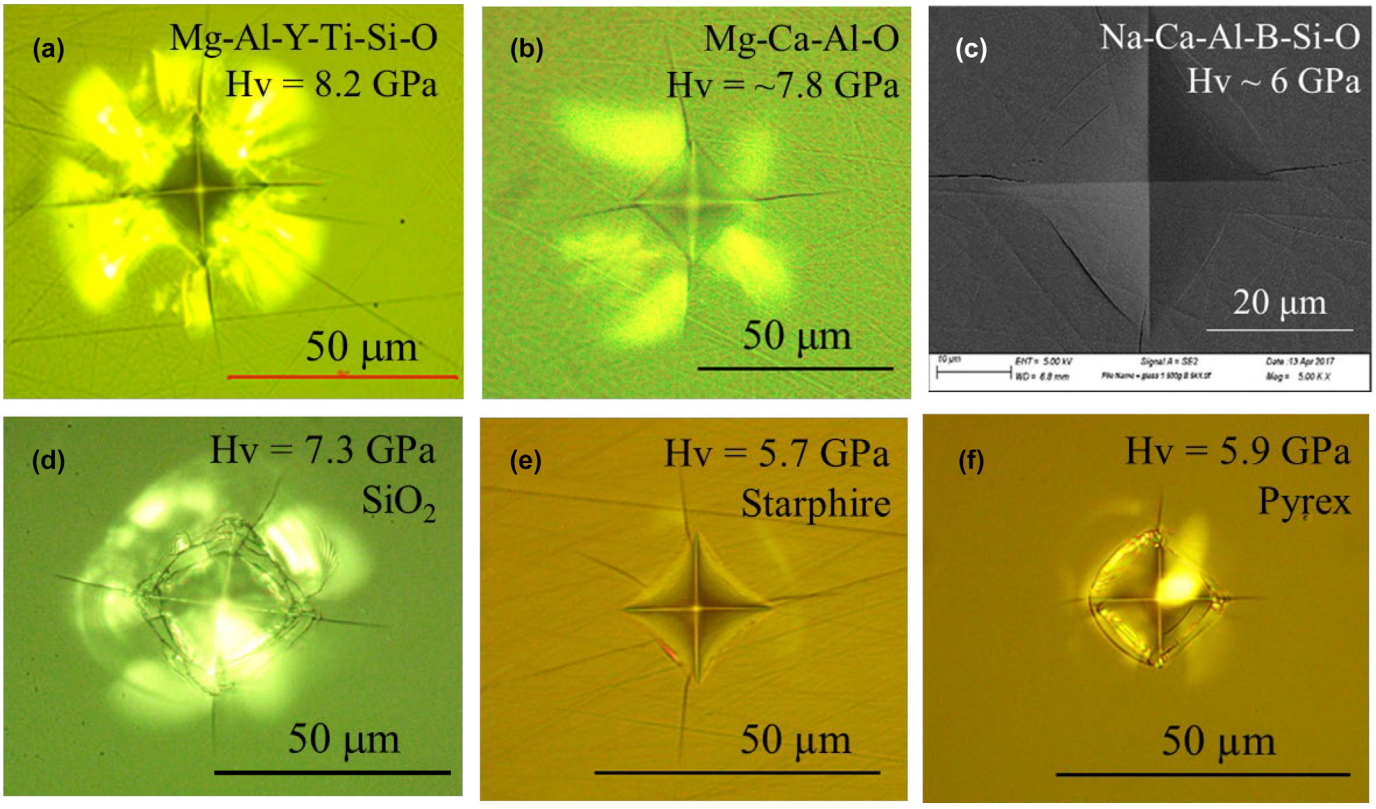


**FIG. 1**

Vickers indent (optical microscope) images of glasses with compositions (mol.%) **(a)** 25.0 MgO- 0.2 CaO- 20.5 $Al_2O_3$ – 12.4 $Yb_2O_3$ – 6.2 $TiO_2$ – 35.7 $SiO_2$ (at 500 gf; 4.90 N); **(b)** 10 MgO – 47.33 CaO – 41.67 $Al_2O_3$ at 4.90 N (4.90 N) load. Both the glasses exhibit $H_v$ in the range of 7.8–8.2 GPa at 1.96 N load. However, both the glasses crack at 4.9 N Vickers load; **(c)** SEM image of Vickers indent in glass with composition 10 $Na_2O$ – 10 CaO – 15$Al_2O_3$ – 5 $B_2O_3$ – 60 $SiO_2$ (mol. %) at 4.90 N load. The glass exhibits the hardness of 5.7 GPa at 1.96 N (200 gf) load, but cracks at 4.90 N load; Optical microscope images of Vickers indent on **(d)** silica glass at 2.94 N (300 gf); **(e)** Starphire and **(f)** Pyrex glass at 1.96 N load.

These studies are disruptive not only because they challenge the long-believed perceived notions, but they also invalidate the proposed correlations between the ICR of oxide glasses and their physical properties. For example, Sellappan et al. [10] proposed a correlation between the Poisson's ratio ($v$) and the ICR of oxide glasses as: $0.15 \leq v \leq 0.20$ – crack resistant; $0.20 \leq v \leq 0.25$ – semi-crack resistant; and $0.25 \leq v \leq 0.30$ – easily damaged. Since the glass 60 $Al_2O_3$ – 40 $SiO_2$ (mol.%) has $v = 0.274$, based on the correlation proposed by Sellappan et al. [10], this glass should exhibit low ICR, which is not the case.

One salient feature that has been highlighted by the studies of Rosales-Sosa et al. [8] and Ke et al. [9] is that in order to achieve a hard and crack resistant glass (when subjected to Vickers indentation), the composition has to be $Al_2O_3$-rich. While the high hardness of $Al_2O_3$-rich glasses has been previously reported [11] and is usually attributed to the increased rigidity in the glass network [12], the high ICR of these glasses can be attributed to the multiple coordination (four, five and six) environments of Al atoms and the mid-range structure around these units, which probably play a role in their shear deformation process [8,9]. Nevertheless, though scientifically intriguing, the concept of $Al_2O_3$-rich glasses poses two significant technological challenges that hinder their translation from laboratory to industry: (1) high processing temperatures and (2) small glass-forming regions. All the hard and crack-resistant $Al_2O_3$-rich glasses reported in the literature [8,9,11,13] exhibit small glass forming regions (near the eutectic) and require processing temperatures >2000 °C. Therefore, to translate the concept of "hard and crack-resistant" glass from the laboratory to industry, glass compositions need to be designed that (1) can be processed at temperatures ≤1700 °C (upper limit of the conventional glass melting furnaces), (2) exhibit minimal tendency towards crystallization during cooling from melt stage, and (3) are chemically durable. The pursuit of accomplishing this goal has witnessed a considerable effort in the past five years where the elastic and mechanical properties of several glass systems in alkali/alkaline-earth aluminosilicate, aluminoborate, and aluminate families have been investigated and correlated with their short-to-medium range structure [5–7,9,14–17]. However, most glasses followed the same suite, i.e., high ICR and low hardness or vice–a–versa.

Although the glass community has not succeeded in accomplishing the goal so far, the knowledge gained from their studies allowed us to infer that to design a hard and crack resistant glass, we need a rigid glass structure with self-adaptive networks, where the rigidity will enhance the hardness, while the self-adaptive networks will accommodate the stress, when subjected to external force, by allowing the change in chemical bonding environment in the structure. Accordingly, the rationale for the design of an industrially scalable, hard, and crack-resistant glass is described below.

1. Previous results pertaining to high $Al_2O_3$ glasses have highlighted that the glass structure needs to have a comparable fraction of four, five and six-coordinated $Al^{3+}$ units [8,18]. While, at one end, the higher coordination of $Al^{3+}$ units will increase the rigidity of the glass network [7,12], thus, increasing its hardness, the possibility of switch in the coordination of $Al^{3+}$ from four to five or six when under deformation load provides the property of self-adaptivity to the glass network [8,9]. Thus, the glass composition is expected to be peraluminous in nature, i.e., alkali/alkaline-earth oxide – to – $Al_2O_3$ ratio is less than 1.
2. The choice of non-framework cation must be made based on its expected role in the glass structure. Alkali cations are known to either act as network modifiers, i.e., create non-bridging oxygens (NBOs), or charge compensators for $AlO_4^-$ and $BO_4^-$ units. Here it should be noted that the presence of NBOs in the silicate or borate network of the glass structure is known to facilitate the isochoric shear flow, resulting in subsurface shear faulting damage [19,20]. On the other hand, the presence of four coordinated boron or aluminum in the glass structure has been shown to be detrimental for achieving the enhanced scratch resistance in glasses [21]. Therefore, alkali oxides are not the most suitable choice for the non-framework cations in this case. According to Logardo et al. [22], the design of a glass with high crack resistance requires reduced fraction of $BO_4^-$ units, fewer Si–O–Al linkages, and more distorted local environment around tetrahedral aluminum. Further, to accomplish the overarching goal, we need a cation that can (somewhat) behave like $Al^{3+}$, i.e., switch between the roles of network former, modifier, and charge compensator. This will help in developing networks that can adapt themselves under the deformation load. These structural attributes can be achieved by selecting an alkaline-earth cation with high ionic field strength, for example, $Be^{2+}$ or $Mg^{2+}$, as the non-framework cation. Considering the challenges associated with beryllium toxicity [23], $Mg^{2+}$ has been chosen as one of the non-framework cations for the design of the glass in the present study. To start with, $Mg^{2+}$ can behave like $Al^{3+}$ by forming $MgO_{4/2}^{2-}$ species, thus, linking to the other network formers via four bridging oxygens, for example, $SiO_4$–$MgO_4$ linkages [21,22,24], while it can also behave as a network modifier similar to $Ca^{2+}$ depending on the local environment in the glass [24]. Further, $Mg^{2+}$ has been shown to reduce the fraction of Si–O–Al linkages and $BO_4^-$ units in the glass structure (compared to $Na^+$) [22].
3. Based on the above discussion, the glass is expected to be designed in the peraluminous region of the MgO–$Al_2O_3$–$SiO_2$ ternary system. However, the peraluminous glasses in this system exhibit poor glass forming ability (high tendency towards crystallization) and high processing temperatures (>2000 °C) [9,25]. Therefore, $B_2O_3$ has been incorporated in the glass structure to lower the processing temperatures and improve the glass forming ability. Also, owing to the peraluminosity of the designed glass composition, the majority of boron is expected to be present in trigonal coordination, i.e., $BO_3$ units, which, in turn, is expected to favor densification during indentation, thus, enhancing the crack resistance [6,7,26]. Here it needs to be emphasized that high concentrations of $B_2O_3$ can be detrimental for the chemical durability of the glass [27,28]. Therefore, the concentration of $B_2O_3$ needs to be optimized to find a correct balance between processing temperatures, mechanical properties, and durability.
4. Finally, the glass forming ability of the designed glass system has been further enhanced by the addition of a rare-earth oxide ($RE_2O_3$, for example, $Y_2O_3$ or $La_2O_3$) to the composition. The addition of rare-earth oxide has been made based on the 'principle of confusion,' – the addition of more components with different ionic field strengths decreases the immiscibility gap, i.e., increases the glass forming ability [29]. According to Mysen and Richet [30], the oxide glasses with large compositional complexity have large entropy of mixing. Therefore, the loss of entropy from the melts of these systems is slow, thereby, increasing their glass forming ability, thus, supporting the validity of 'confusion principle' in the design of oxide glasses. Since the glasses in the MgO-$Al_2O_3$-$B_2O_3$-$SiO_2$ are known to phase separate into borate and silicate-rich networks [31], the addition of $RE^{3+}$ is expected to minimize the immiscibility gap and enhance the glass forming ability of the system. Additionally, due to their high ionic field strength, rare-earth cations are expected to push $Al^{3+}$ in five and six-coordination, thus facilitating the formation of oxygen triclusters, which have been recently shown to promote high indentation crack resistance in oxide glasses [32].

Accordingly, the present study reports a hard and crack-resistant glass designed in the peraluminous region of MgO–$Al_2O_3$–$Y_2O_3$–$B_2O_3$–$SiO_2$ (hereafter labeled as RU glass), where the molar ratio of $Al_2O_3/(MgO + Y_2O_3) \geq 1.75$, $Al_2O_3 > 30$ mol %, and $B_2O_3 < 20$ mol.%.

## Experimental

### *Glass synthesis*

The RU glass has been synthesized by the conventional melt-quench technique wherein a batch comprising high purity (>99.0 %) oxides and carbonates corresponding to 150 g glass has been melted in a Pt-Rh crucible (loosely covered with a Pt lid) at 1625 °C for 1 h followed by quenching of melt on a metallic plate and annealing at 550 °C for 1 h. Multiple batches (up to 300 g) of the same composition were melted following the same methodology to ascertain the reproducibility of the results. The annealed glass was analyzed using X-ray diffraction (XRD; Cu $K_\alpha$; $2\theta$ = 10–90°; PANalytical – X'Pert Pro; step size: 0.01313° $s^{-1}$) to confirm its amorphous nature, while an agreement between the batched and experimental composition of the glass was confirmed by the inductively coupled plasma – optical emission spectroscopy (ICP-OES, Optima 8000, Perkin Elmer), as shown in Table 1.

To compare the properties of RU glass with the commercial glasses, Starphire® (mol.%., 14.31 $Na_2O$ – 0.01 $K_2O$ – 0.12 MgO – 11.06 CaO – 0.12 SrO – 0.86 $Al_2O_3$ – 0.01 $ZrO_2$ – 73.52 $SiO_2$ [33]) glass was synthesized following the above-described methodology. The glass was annealed at 500 °C for 1 h. Pyrex/Borofloat glass (mol.%, 4.0 $Na_2O$ – 1.4 $Al_2O_3$ – 11.6 $B_2O_3$ – 83.0 $SiO_2$ [34]) and silica ($SiO_2$) glass were purchased from McMaster-Carr (Codes: 8476 K32; 7784 N11). Further, the glasses discussed in Fig. 1**(a–c)**

**TABLE 1**

**Batched and experimental composition (mol.%) of the RU glass.**

| | Batched | Experimental |
|---|---|---|
| MgO | 10.0 | 11.0 ± 1.3 |
| $Y_2O_3$ | 9.6 | 9.9 ± 0.7 |
| $Al_2O_3$ | 34.9 | 35.1 ± 0.4 |
| $B_2O_3$ | 15.5 | 15.9 ± 1.3 |
| $SiO_2$ | 30.0 | 28.2 ± 1.0 |

were synthesized in the laboratory by melt-quench technique followed by annealing at temperatures ~ 50 °C below their respective glass transition temperatures (as measured by the differential scanning calorimeter – DSC).

### *Structure of RU glass*

The density of the glass (at room temperature) was measured by Archimedes' method. D-Limonene was used as the immersion liquid and a digital balance of sensitivity $10^{-4}$ g was employed to weigh the glass samples. The density data presented here is an average of nine measurements (3 samples × 3 measurements per sample). The density of the sample was calculated using Eq. (1),

$$\rho = \frac{m_d}{(m_d - m_s)} \times \rho_s \tag{1}$$

where, $\rho_s$ is the density of the solution (limonene; 0.8411 g/cm$^3$), $m_d$ and $m_s$ is the mass of the sample in air and limonene respectively.

The atomic packing density ($C_g$) of glass, defined as the ratio between the minimum theoretical volume occupied by the ions and the experimental molar volume of the glass, has been calculated using Eq. (2),

$$C_g = \rho \frac{\sum f_i V_i}{M} \tag{2}$$

where, $\rho$ is the experimental density of the glass, $M$ is the molar mass of the glass, $f_i$ is the molar fraction of oxide $i$, and $V_i$ is the ionic volume of oxide $i$. The ionic volume is given by $V_i = \frac{4}{3}\pi N(x{r_A}^3 + y{r_B}^3)$, where $N$ is the Avogadro number, $x$ and $y$ are the number of atoms in the $A_xB_y$ oxide, $r_A$ and $r_B$ are the ionic radii of cations and anions, respectively, which are taken from Shannon [35].

Single resonance $^{27}$Al, $^{11}$B MAS NMR spectra were recorded on a 14.1 T Varian DD2 600 MHz spectrometer using a commercial 4.0 mm MAS NMR probe (Agilent). The powdered samples were packed into 4.0 mm zirconia rotors and spun at 12 kHz for $^{27}$Al and 10 kHz for $^{11}$B. $^{27}$Al MAS NMR spectra were measured at 156.27 MHz with π/6-pulse durations of 0.8 μs and recycle delays of 1 s. Measurements were signal-averaged over at least 580 scans and were processed without additional line broadening. $^{11}$B MAS NMR spectra were measured at 192.40 MHz with π/6-pulse durations of 0.9 μs and recycle delay of 8 s. Measurements were signal-averaged over at least 120 scans and were processed without additional line broadening. Chemical shifts of $^{27}$Al are reported relative to powdered $AlPO_4$ (measured at 40.7 ppm relative to a 1 M aqueous solution of $Al(NO_3)_3$), and $^{11}$B chemical shifts are reported relative to powdered $BPO_4$ (measured at −3.5 ppm relative to an aqueous solution of $BF_3$ .$Et_2O$).

### *Elastic and mechanical properties*

The glass samples were ground and polished using non-aqueous diamond grit suspensions to obtain optically flat surface for microhardness testing. Vickers hardness ($H_v$) up to 19.6 N was measured using a Vickers micro-indenter, Leco LM-248AT, while Leco LV110 indenter was used to measure the hardness at loads ≥29.4 N. The measurements were performed in air at room temperature (Relative Humidity: 32 %) with a dwell time of 10 s. Twenty-five indentations at each load (0.98 N, 1.96 N, 2.9 N, 4.9 N, 9.8 N, 19.6 N, 29.4 N, and 49 N) were performed. Samples were spaced according to ASTM C1327-15, after crack length was established with a test indent. The indentation feature measurement was performed digitally on images of indents at 50× magnification using an OMAX A35140U3 14.0MP camera and its associated software, TopView. Eq. (3) was used to calculate the $H_v$, where $P$ is the indentation load (N) for median cracking, $\alpha$ is a shape parameter (2 for Vickers indenter), and $a$ is the half-diagonal length of the indent.

$$H_V = \frac{P}{\alpha a^2} \tag{3}$$

To ascertain the likelihood of crack initiation resistance at a specific load, the average number of cracks per indent were divided by four (defined as crack probability), representing the maximum potential number of radial cracks per Vickers indent (equivalent to the number of corners). This calculation was performed over a range of loads (mentioned above), spanning from minimal loads with no radial cracking (0 % crack initiation probability) to higher loads resulting in extensive cracking (100 % crack probability). Subsequently, a suitable mathematical function was applied to the data. The load at which the probability of median/radial cracks originating from the four corners of the Vickers indent impression reaches 50 % is defined as indentation crack resistance (ICR) of a glass [36]. Please note that the term "indentation crack resistance" used here is similar (but not equivalent) to the term "contact damage resistance" used to study the propensity of crack formation in ceramics when subjected to indentation [37].

Elastic moduli (e.g., Young's, bulk and shear modulus and Poisson's ratio) of the RU glass were measured by Brillouin light scattering (BLS). The glass samples were cut into approximately 10 mm × 10 mm in size by a low-speed diamond saw. They were then optically polished to 500–800 μm in thickness with parallel top and bottom surfaces by using 600 grit SiC sand paper and non-aqueous diamond grit suspension. A six-pass high contrast Fabry–Perot interferometer from the JSR Scientific Instruments was used to carry out BLS measurements. A 532 nm Verdi V2 DPSS green laser was used as the probing light source. Brillouin spectra were collected in the emulated platelet geometry (EPG). The details of the experimental set up and the light scattering geometry can be found elsewhere [38]. From the measured longitudinal ($V_L$) and transverse sound ($V_T$) velocities in Brillouin scattering, together with density ($\rho$), shear modulus ($G$), Young's modulus ($E$), Bulk modulus ($K$) and Poisson's ratio ($\nu$) can be calculated using the following equations:

$$C_{11} = \rho V_L^2 \tag{4}$$

$$G = C_{44} = \rho V_T^2 \tag{5}$$

$$E = C_{44}\frac{3C_{11} - 4C_{44}}{C_{11} - C_{44}} \quad (6)$$

$$v = \frac{E}{2G} - 1 \quad (7)$$

$$K = \frac{E}{3(1-2v)} \quad (8)$$

The elastic properties of Starphire, Pyrex/Borofloat, silica, Eagle® XG, Lion Glass and cesium aluminoborate glass, reported in Table 2, have been obtained from the literature [5,33,39] or their technical specification sheets provided by their respective manufacturers.

### *Thermal and optical properties*

The glass transition temeparture ($T_g$) of all the glasses synthesized in the laboratory was measured using a Simultaneous Thermal Analyzer (NETZSCH 449 F5 Jupiter, Burlington, MA) in the temperature range of 100 °C–1000 °C at a heating rate of 20 °C/min under a constant flow of nitrogen gas. ~30–40 mg glass powder (particle size: < 45 μm) was loaded in a Pt pan with an empty Pt pan being used as a reference. The DSC data reported for any glass composition are an average of at least three thermal scans.

The refractive index of the RU glass (optically polished to 500–800 μm in thickness) was measured using a Metricon Model 2010/M Prism Coupler with an accuracy of ± 0.0002. The optical transmittance of the glass in the wavelength region of 200 nm – 2400 nm was measured on samples with thickness varying between 500 μm – 800 μm using an automated reflectance and transmittance measurement system (LAMBDA 950; Perkin Elmer). The data presented in the article is an average of measurements taken on at least three different samples.

## Results and discussion

Fig. 2 shows the X-ray diffraction patterns of RU glass, Starphire, silica and Pyrex. The XRD patterns of all the glasses depict a broad hump, thus confirming their amorphous nature. Fig. 3 shows the images of the RU glass with approximate dimensions: 50 mm × 45 mm × 7 mm demonstrating its ease of processing and scalability. Here it needs to be emphasized that the polished glass specimen shown in Fig. 3 has been cut from a larger piece of glass with approximate dimensions: 100 mm × 100 mm × 8 mm.

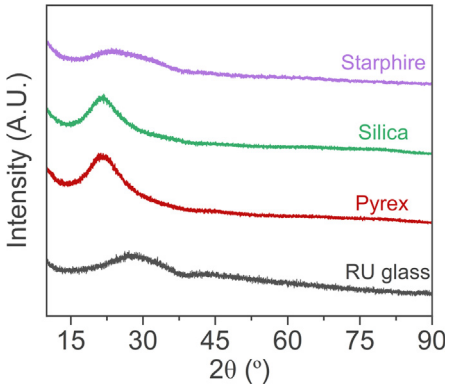


**FIG. 2**

X-ray diffractograms of RU glass, Pyrex, Silica and Starphire glass.

The glass transition temperature (onset) of the RU glass is 766 ± 7 °C **(**Fig. 4**)**, while its the density and refractive index are 3.005 ± 0.003 g/cm$^3$ and 1.636 ± 0.001, respectively **(**Table 2**)**. The optical transmittance of the glass in the wavelength region of 200 nm–2400 nm is 90 ± 2 %, comparable to the other commercial glasses, as shown in Fig. 5.

Since 1D MAS NMR spectroscopy can decipher the coordination number of different network forming moieties (e.g., $B^{3+}$, $Al^{3+}$, $P^{5+}$, etc.) in the glass structure, it can be used as a qualitative tool for predicting and understanding the structural response of the glass to sharp contact loading. Therefore, we have probed the short-range order using $^{11}B$ and $^{27}Al$ MAS NMR spectroscopy to understand the structural origins of high ICR of the RU glass in the present investigation. The $^{11}B$ MAS NMR **(**Fig. 6**a)** reveals ~90 % boron atoms to be three-coordinated ($B^{III}$) in the glass structure, while remaining boron atoms being in four-coordination ($B^{IV}$). Similarly, the $^{27}Al$ MAS NMR spectra of the RU glass **(**Fig. 6**b)** reveals ~47 % of aluminum atoms to be four-coordinated ($Al^{IV}$), ~43 % are five-coordinated ($Al^{V}$) and the rest ~10 % are present in six-coordination ($Al^{VI}$).

The Young modulus (E), shear modulus (G) and Bulk modulus (K) of the RU glass have been measured/calculated to be 112.56 ± 0.37 GPa, 43.68 ± 0.19 GPa, and 88.70 GPa respectively. These values are significantly higher than those of most commercial glasses designed over a broad composition space, as shown in

**TABLE 2**

**A comparison of physical, elastic, and mechanical properties of several commercial and non-commercial oxide glasses with the RU glass.**

| Glass | Bulk modulus (GPa) | Young's modulus (GPa) | Shear modulus (GPa) | Poisson's ratio | Refractive index | Density (g/cc) | Vicker's Hardness (GPa) | Indentation Crack Resistance (N) |
|---|---|---|---|---|---|---|---|---|
| RU glass | 88.70 ± 0.24 | 112.56 ± 0.37 | 43.68 ± 0.19 | 0.288 ± 0.001 | 1.640 ± 0.001 | 3.005 ± 0.003 | 7.84 ± 0.047 | 26.5 |
| Pyrex | 34.00 ± 0.47 | 61.02 ± 0.52 | 25.41 ± 0.36 | 0.200 ± 0.070 | 1.475 ± 0.002 | 2.216 ± 0.001 | 5.96 ± 0.046 | 4.0 |
| Starphire | 43.22 ± 0.25 | 71.48 ± 0.23 | 29.19 ± 0.11 | 0.224 ± 0.002 | 1.525 ± 0.003 | 2.496 ± 0.002 | 5.74 ± 0.036 | 2.7 |
| Borofloat®33 | 35.5 | 64.0 | 26.7 | 0.20 | 1.471 | 2.23 | 5.51 | 6.9 |
| Silica | 36.7 | 72.0 | 31.2 | 0.17 | 1.470 | 2.20 | 7.30 | 2.9 |
| Eagle® XG | 45.4 | 73.6 | 30.1 | 0.23 | 1.598 | 2.38 | 6.27 | – |
| Cs-Al-B | 13.3 | 20.0 | 8.0 | 0.25 | – | 2.89 | 2.00 | 30.0 |
| Lion Glass‡ | ~41.5 | ~60.3 | ~24.0 | ~0.26 | – | ~2.74 | 4.37–5.62 | 0.98 – >9.8 |

‡ Lion Glass is a multicomponent phosphate glass.

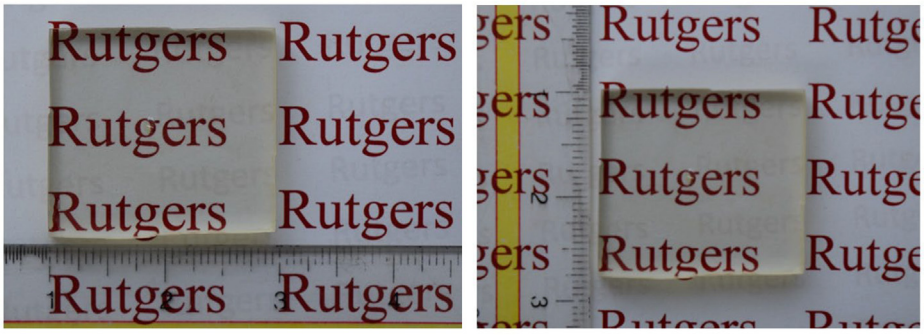


**FIG. 3**

RU glass with approximate dimensions: 50 mm × 45 mm × 7 mm demonstrating its ease of processing and scalability. The glass pieces have been cut and polished (in non-aqueous media) from samples with ~10 cm diameter and ~ 8–10 mm thickness.

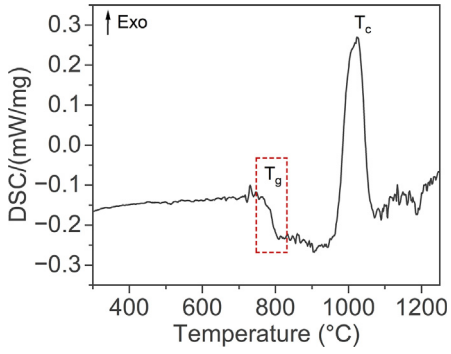


**FIG. 4**

DSC thermograph of RU glass.

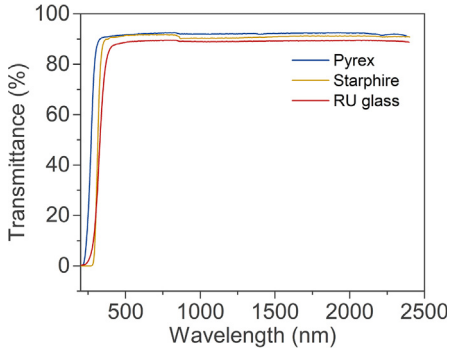


**FIG. 5**

The optical transmittance spectrum of RU glass, Pyrex and Starphire glass in the wavelength region of 200 nm–2400 nm, as measured on samples with thickness varying between 500 μm–800 μm.

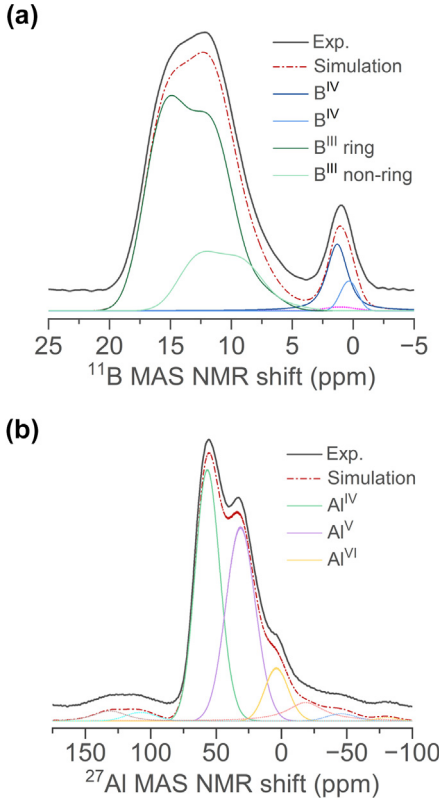


**FIG. 6**

**(a)** $^{11}$B and **(b)** $^{27}$Al MAS NMR spectra of RU glass. The $^{11}$B MAS NMR spectrum was fitted with two Q MAS1/2 components for $B^{III}$ resonance and three Gauss/Lorentz functions for $B^{IV}$ resonances. The minor dotted fitted peak displayed near 0 ppm represents the central peak of the satellite transition manifold of $B^{IV}$ resonances, which overlaps with the MAS peaks of the central transition, and whose area needs to be considered when extracting $N_4$ values from the spectra. The $^{27}$Al MAS NMR spectra was fitted using CZ simple method for $Al^{IV}$, $Al^{V}$ and $Al^{VI}$ components (showed in solid lines) and the side bands are fitted using the Gauss/Lorentz function (showed in dotted lines).

Table 2, thus, opening a possibility for their application as high modulus glass fibers in advanced composites.

Further, as per the correlation between the Poisson's ratio ($\nu$) and the ICR of oxide glasses proposed by Sellappan et al. [10], the RU glass should exhibit low ICR (easily damaged) as its Poisson's ratio ($\nu$) is 0.288. However, the RU glass exhibits Vickers hardness of 7.84 ± 0.47 GPa (at 1.96 N) and ICR of 26.5 N, as shown in Fig. 7. Figs. 8 and 9 present the images of the Vickers indents on RU glass at 9.8 N and 19.6 N, respectively, thus corroborating the data presented in Fig. 7. The values of $H_v$ and ICR of the RU glass are significantly higher than those of most commercial or non-commercial glasses (prior to thermal tempering, densification near $T_g$, or chemical strengthening), as shown in Table 2 and Fig. 10 [plotted using data from Ref. 5-7, 14, 16,

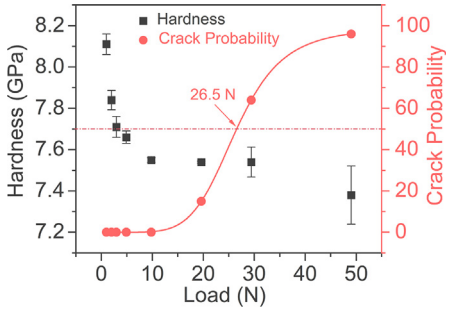


**FIG. 7**

Vickers's hardness and crack probability as a function of applied indentation load for the RU glass.

26, 40–43]. Further, when compared to the literature, the $H_v$ of the RU glass is comparable to the peraluminous $MgO–Al_2O_3–SiO_2$ based glasses synthesized by Ke et al. [9] using aerodynamic levitation technique and the 60 $Al_2O_3$ – 40 $SiO_2$ glass reported by Rosales-Sosa et al. [8]. Although the ICR of the RU glass (26.7 N) is comparatively lower than that reported for 11.15 MgO – 38.39 $Al_2O_3$ – 50.00 $SiO_2$ glass (CR ≈ 50 N) by Ke et al. [9], the latter composition is not amenable for processing under the conventional industrial infrastructure due to the requirement of high temperatures and low glass forming regions, as discussed above.

Like $v$, $C_g$ is also known to play a predominant role in the cracking behavior of oxide glasses, where a low value of $C_g$ translates into glasses with high resistance to cracking. In general, the $C_g$ of oxide glasses varies between 0.4 and 0.6, wherein, glasses with lower $C_g$ tend to exhibit high ICR (due to their ability to densify under load) and low $H_v$ [44], and vice-versa, as shown in Fig. 10a and 10b, respectively. The only exception to the trend of ICR vs. $C_g$ are a few glasses from alkali/alkaline earth aluminoborate family. However, all these glasses exhibit the known inverse relationship between CR and $H_v$ (Fig. 10c).

In the above discussed context, the RU glass has a high $C_g$ value of 0.54, which means it is structurally compact and is expected to possess high Vicker's hardness. However, the ambiguity here is its high ICR (of 26.5 N), which is contradictory to the trends of ICR vs. $C_g$ of borosilicate and aluminoborosilicate families, presented in Fig. 10. Therefore, the parameters pertaining to the amount of free volume in the glasses cannot be the guiding principle in defining or predicting the cracking behavior in the oxide glasses.

Since the cracking behavior of glass under sharp contact loading depends on the stress/residual stress buildup during the loading and unloading process, the high resistance of the RU glass to cracking can be explained by the ability of the atomic network to undergo stress induced reversible and irreversible changes in bond lengths, bond angles, and coordination numbers

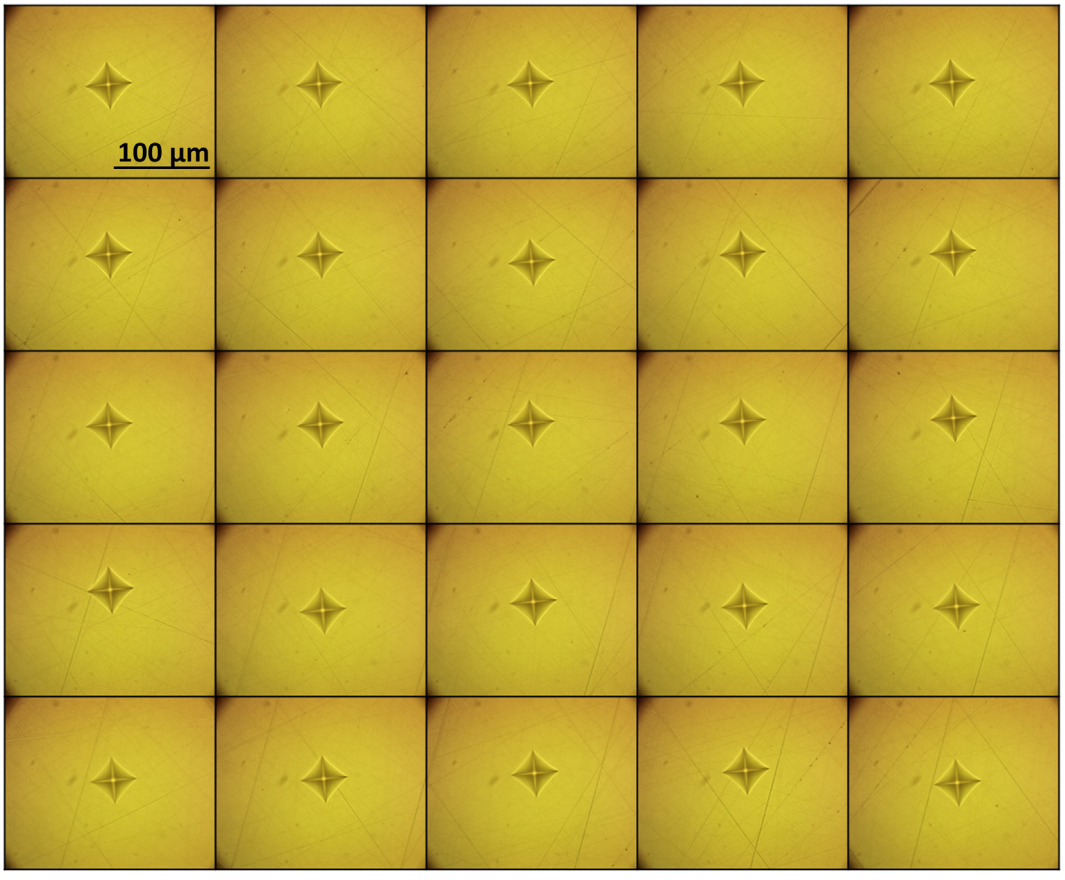


**FIG. 8**

Optical images of 25 indents produced at the indentation load of 9.8 N on the surface of the RU glass. The size of the images is 180 µm × 220 µm.

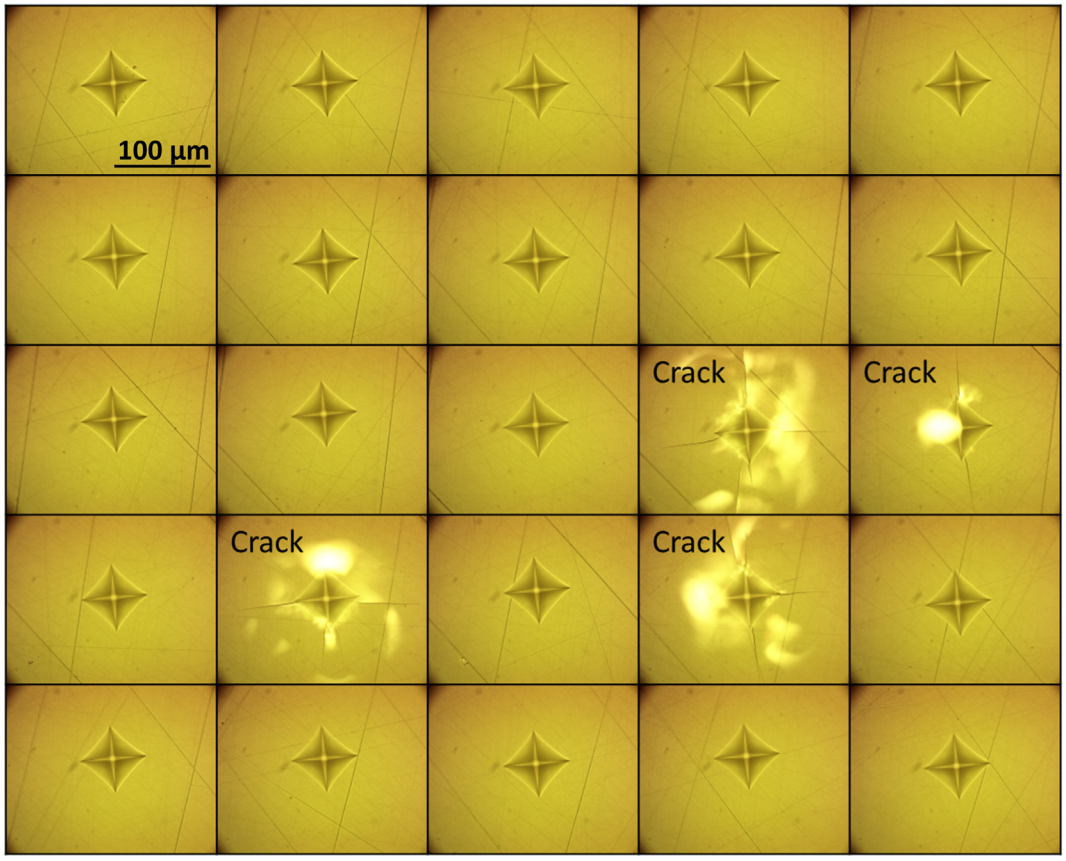


**FIG. 9**

Optical images of 25 indents produced at the indentation load of 19.6 N on the surface of the RU glass. The size of the images is 180 μm × 220 μm.

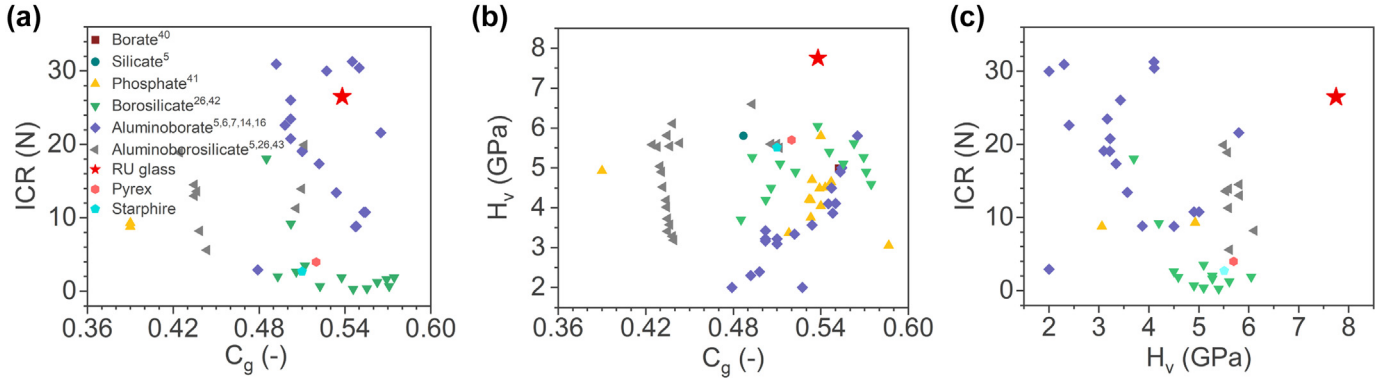


**FIG. 10**

Correlation between **(a)** ICR and $C_g$, **(b)** $H_v$ and $C_g$, and **(c)** ICR and $H_v$, for different oxide glasses and the RU glass. The data plotted in this figure has been sourced from the following references: [5–7,14,16,26,40–43].

[8,21,22]. Each of these structural changes in glass results in stress adaptability and has an associated energy cost which decides its preferential response. For instance, increasing the coordination number of Si atoms requires significant activation energy. Hence, silicate glasses typically densify under load through a decrease of the inter-tetrahedral Si—O—Si angle and/or change in ring size distribution [45–47]. This results in a low self-adaptivity in multicomponent silicate glasses, leading to lower ICR values. In contrast, the energy associated with the transformation of $B^{III}$ to $B^{IV}$ is significantly lower than the Si and Al counterparts, i.e., glasses with high fraction of $B^{III}$ units tend to exhibit high ICR [6].

In the present case, the RU glass is expected to respond to sharp contact loading by a discernible shift in B coordination, transitioning from trigonal to tetragonal coordination along with an evident adjustment in Al coordination, progressing from 4-fold to 5-fold, and occasionally attaining 6-fold coordination [6,48]. Furthermore, the $B^{III}$ structural units (accounting for

90 % of the boron network) present in the glass may further respond to sharp contact loading by demonstrating increased shear deformation as seen in earlier investigations [48]. These dual mechanisms have been reported to significantly contribute to the densification and subsequent dissipation of stress during loading in the case of aluminoborate glasses [6]. Finally, it's crucial to acknowledge the significant role played by oxygen triclusters in peraluminous glasses as an additional mechanism for dissipating energy during indentation. As per a recent study by Shan et al. [32], the bonds within three-coordinated oxygen triclusters exhibit greater ionic character, making them weaker and more flexible in comparison to two-coordinated bridging oxygens (BO). Upon mechanical loading and unloading, these oxygen tri-clusters undergo more facile bond breaking-closing process. This localized process effectively dissipates mechanical energy, thereby leaving minimal energy for the rupture of breaking rigid bonds, i.e., BO–Si, consequently preventing crack initiation and propagation. Nonetheless, it needs to be emphasized that though the presence of oxygen triclusters in RU glass is highly likely owing to its peraluminous nature and presence of high field strength cations ($Mg^{2+}$, $Y^{3+}$), their presence and quantification needs experimental validation.

To summarize, the higher ICR of RU glass stems from the diminished accumulation of stress during loading and the subsequent decrease in residual stress buildup after unloading, thereby lowering the driving force for crack formation.

## Conclusions

We report a glass with high hardness and indentation crack resistance that can be synthesized and scaled-up in the conventional industrial infrastructure. The structural design of the glass has been described and experimentally validated. The results presented here are not only scientifically intriguing but have considerable tangible implications, as they pave the path for the design and development of stronger glasses for functional applications.

## Credit authorship contribution statement

**Anjali Yadav:** Writing – review & editing, Methodology, Investigation, Data curation, Formal analysis. **Anne Rebecca:** Data curation. **Saurabh Kapoor:** Writing – review & editing, Formal analysis. **Yueh-Ting Shih:** Data curation. **Liping Huang:** Writing – review & editing, Resources, Data curation. **Ashutosh Goel:** Writing – review & editing, Writing – original draft, Supervision, Resources, Project administration, Methodology, Investigation, Funding acquisition, Formal analysis, Conceptualization.

## Data availability

Data will be made available on request.

## Declaration of competing interest

The authors declare that they have no known competing financial interests or personal relationships that could have appeared to influence the work reported in this paper.

## Acknowledgement

This material is based upon work supported by the Rutgers TechAdvance® Fund (TA2020-0332), National Science Foundation under Grants No. 2034871 and 1936368, and Ceramic, Composite and Optical Materials Center at Rutgers University. The authors would like to thank Dr. Nicholas Stone-Weiss and Prof. John McCloy from Washington State University for helping with MAS NMR spectroscopy data acquisition, and Mr. Christopher Lynch from PerkinElmer, Inc. for help with collecting the transmission spectra of the RU glass.

### References

[1] L. Wondraczek et al., Adv. Mater. (2022) 2109029.
[2] L. Wondraczek et al., Adv. Mater. 23 (39) (2011) 4578–4586.
[3] M.M. Smedskjaer, J.C. Mauro, Y.Z. Yue, Phys. Rev. Lett. 105 (2010) 11.
[4] M. Bauchy et al., Phys. Rev. Lett. 114 (12) (2015) 125502.
[5] K. Januchta et al., Adv. Sci. 6 (18) (2019) 1901281.
[6] K. Januchta et al., Chem. Mater. 29 (14) (2017) 5865–5876.
[7] K. Januchta et al., J. Non Cryst. Solids 460 (2017) 54–65.
[8] G.A. Rosales-Sosa et al., Sci. Rep. 6 (2016) .
[9] X. Ke et al., J. Am. Ceram. Soc. 103 (6) (2020) 3600–3609.
[10] P. Sellappan et al., Acta Mater. 61 (16) (2013) 5949–5965.
[11] A. Rosenflanz et al., Nature 430 (7001) (2004) 761–764.
[12] M. Ren et al., J. Non Cryst. Solids 505 (2019) 144–153.
[13] G.A. Rosales-Sosa et al., J. Am. Ceram. Soc. 101 (11) (2018) 5030–5036.
[14] K.F. Frederiksen et al., J. Phys. Chem. B 122 (23) (2018) 6287–6295.
[15] N. Mascaraque et al., J. Non Cryst. Solids 499 (2018) 264–271.
[16] K. Januchta et al., Phys. Rev. Mater. 1 (2017) 6.
[17] M.M. Sebdani et al., J. Non Cryst. Solids 427 (2015) 160–165.
[18] T.K. Bechgaard et al., J. Non Cryst. Solids 441 (2016) 49–57.
[19] K.W. Peter, J. Non Cryst. Solids 5 (2) (1970) 103–115.
[20] A. Arora et al., J. Non Cryst. Solids 31 (3) (1979) 415–428.
[21] H. Bradtmuller et al., J. Phys. Chem. C 123 (24) (2019) 14941–14954.
[22] M. Lograd et al., J. Am. Ceram. Soc. 104 (5) (2021) 2250–2267.
[23] M.R. Buchner, Zeitschrift Für Naturforschung B 75 (5) (2020) 405–412.
[24] S. Kroeker, J.F. Stebbins, Am. Mineral. 85 (10) (2000) 1459–1464.
[25] P.F. McMillan, R.J. Kirkpatrick, Am. Mineral. 77 (7–8) (1992) 898–900.
[26] Y. Kato et al., J. Ceram. Soc. Jpn. 118 (1381) (2010) 792–798.
[27] S. Kapoor et al., J. Phys. Chem. B 122 (48) (2018) 10913–10927.
[28] N. Stone-Weiss et al., Acta Biomater. 65 (2018) 436–449.
[29] C. Calahoo, L. Wondraczek, J. Non-Cryst. Solids: X 8 (2020) 100054.
[30] B. Mysen, P. Richet, Silicate glasses and melts: properties and structure, Elsevier, 2005.
[31] N. Bisbrouck et al., J. Am. Ceram. Soc. 104 (9) (2021) 4518–4536.
[32] Z. Shan et al., Acta Mater. 262 (2024) 119425.
[33] A.A. Wereszczak, C.E. Anderson, Int. J. Appl. Glas. Sci. 5 (4) (2014) 334–344.
[34] M.M. Smedskjaer, R.E. Youngman, J.C. Mauro, Appl. Phys. a-Mater. Sci. Process. 116 (2) (2014) 491–504.
[35] R.D. Shannon, Acta Crystallographica A 32 (5) (1976) 751–767.
[36] M. Wada, H. Furukawa, K. Fujita, Proc. Int. Cong. Glass 11 (1974) 39–46.
[37] X. Wang, N.P. Padture, H. Tanaka, Nat. Mater. 3 (2004) 539–544.
[38] M. Guerette, L. Huang, J. Phys. D Appl. Phys. 45 (2012) 275302.
[39] J.C. Mauro, et al., Low-melting glass compositions, articles and methods of making the same, World Intellectual Property Organization (WIPO), Application Number: PCT/US2023/015177.
[40] M.M. Smedskjaer et al., Sci. Rep. 4 (2014) 3770.
[41] S. Kapoor et al., J. Non Cryst. Solids 469 (2017) 31–38.
[42] M.N. Svenson et al., Phys. Rev. Appl 2 (2) (2014) 024006.
[43] X. Ren et al., Materials 14 (13) (2021) 3450.
[44] S. Kapoor et al., Front. Mater. 6 (2019) 63.
[45] J. Sehgal, S. Ito, J. Am. Ceram. Soc. 81 (1998) 2485–2488.
[46] S. Kapoor, L. Wondraczek, M.M. Smedskjaer, Front. Mater. 4 (2017) 1.
[47] M. Guerette et al., Sci. Rep. 5 (2015) 15343.
[48] H. Liu et al., J. Appl. Phys. 128 (2020) 035106.